Moving fronts in entangled polymeric films

Brian M. Besancon and Peter F. Green
Department of Chemical Engineering and Texas Materials Institute, The University of Texas at Austin, Austin, Texas 78712, USA
(Received 26 May 2004; revised manuscript received 2 August 2004; published 22 November 2004)

Thin liquid films can become structurally unstable and dewet, forming holes which subsequently grow on the substrate. Considerable research has been conducted on the structural evolution and growth of holes, which invariably are shown to be circular. We show that morphologies characterized by *circular* holes comprise one of three possible morphological regimes. In polystyrene films, supported by silicon oxide substrates, two other regimes are observed with decreasing film thickness. In the second regime, the moving boundary of the growing hole may become unstable and form fingers. The spacing between the fingers is characterized by a well-defined wavelength $\lambda \propto h^{7/6}M^{-1/2}$, where h is the film thickness and M is the molecular weight. A dense branchlike morphology characterizes the peripheral regions of the holes in the third regime and is found only in the thinnest films.

DOI: 10.1103/PhysRevE.70.051808 PACS number(s): 61.41.+e, 68.08.−p, 68.15.+e

INTRODUCTION

A problematic issue associated with the processing of thin, nonpolar, polymeric liquid films is rupturing and subsequent dewetting of the film from an underlying substrate. It is well known that this phenomenon is particularly active in films with thicknesses h_0 on the order of nanometers or tens of nanometers and its origins are, for the most part, reasonably well understood [1–10]. The excess interfacial free energy of interaction per unit area, $\Delta G(h)$, or equivalently the effective interface potential, between the liquid-substrate interface and the liquid-vapor interface, is determined through the competition between long-ranged van der Waals forces and short-ranged intermolecular forces whereby $\Delta G(h) = \delta(h) - A_{132}/12\pi h^2$ [9,10]. The first term describes the short-range interactions that are associated with molecules in contact (distances less than 1 nm) and is frequently represented by a power law [10] or decaying exponential [9,11]. The second term describes the long-ranged van der Waals interactions [9–11]. The effective Hamaker constant A_{132} is defined in terms of the individual Hamaker constants for the three media vapor (1), polymer (3), and substrate (2) and can be positive or negative. A net attraction exists between these interfaces when A_{132} is positive [12]. Specifically, a disjoining pressure $\Pi = -\partial\Delta G/\partial h = -A_{132}/6\pi h^3$ is created in the film where thinner regions of the film experience greater pressure than thicker regions. Hence a net flow of mass from thinner regions of the film to the thicker regions occurs. The Laplace pressure (ratio of the surface tension to the local radius of curvature) opposes these thickness modulations. The competition between the Laplace pressure and the disjoining pressure dictates a critical wavelength beyond which the fluctuations will grow, characterized by a dominant wave vector $q \propto (-\partial^2\Delta G/\partial h^2)^{1/2}$ [9,10]. This is the process of spinodal dewetting and has been shown to occur in polystyrene (PS) films thinner than 3 nm on silicon substrates with a native oxide layer (hereafter referred to as Si/SiO_x) [10].

For sufficiently thick films beyond the length scale over which the interface potential possesses negative curvature, dewetting occurs via nucleation and subsequent growth of holes [10]. During the nucleation stage, a circular crest forms at the periphery of a depression spontaneously created in the film and the depression penetrates into the film [13,14]. When it impinges on the substrate, capillary driving forces become responsible for growth (negative spreading coefficient) of the hole. A rim subsequently develops around the hole due to the accumulation of chains excavated from the substrate as the hole radius increases.

The vast majority of studies of dewetting films have concentrated on PS thin films supported by Si/SiO_x substrates [3,4,14–18]. Generally, these studies show that a typical hole remains circular during growth [Fig. 1(a)] and that the shape of its rim remains stable. However, fluctuations of the shape of the rim of a growing hole may occur [19] and the rim may subsequently become unstable and form fingers [4,20]. The image in Fig. 1(b) shows the early stage of finger formation in a thin PS film. Masson *et al.* showed that for entangled thin PS films on Si/SiO_x substrates, fingering instabilities occur provided that films are sufficiently thin [20]. The range of film thicknesses over which fingering was observed increased with increasing molecular weight [20]. Reiter and Sharma [21] also showed that fingers developed in the receding edge of polydimethylsiloxane (PDMS) films dewetting from high-density grafted layers of PDMS.

It is generally understood that fingering instabilities occur at the line of contact of a liquid that is forced to spread on a substrate due to external driving forces, such as gravitational forces [22–25], centrifugal forces [26], or Marangoni forces [27] (gradients in surface tension). Fingering instabilities occur when fluctuations at the liquid front are amplified due largely to effects associated with the surface tension γ. For example, when the liquid flows down an incline due to gravity, at a rate faster than it would normally spread due only to capillarity, a rim (sometimes called a "bump") develops at the line of contact [22–25]. The shape of this rim fluctuates so the height of the rim varies from one location to another. Consequently, a Laplace pressure develops, producing surface curvature flows that contribute to local pressure gradients along the rim in order to suppress the fluctuations. Thicker regions of the rim provide less resistance to flow down the incline than the thinner regions. If the driving force

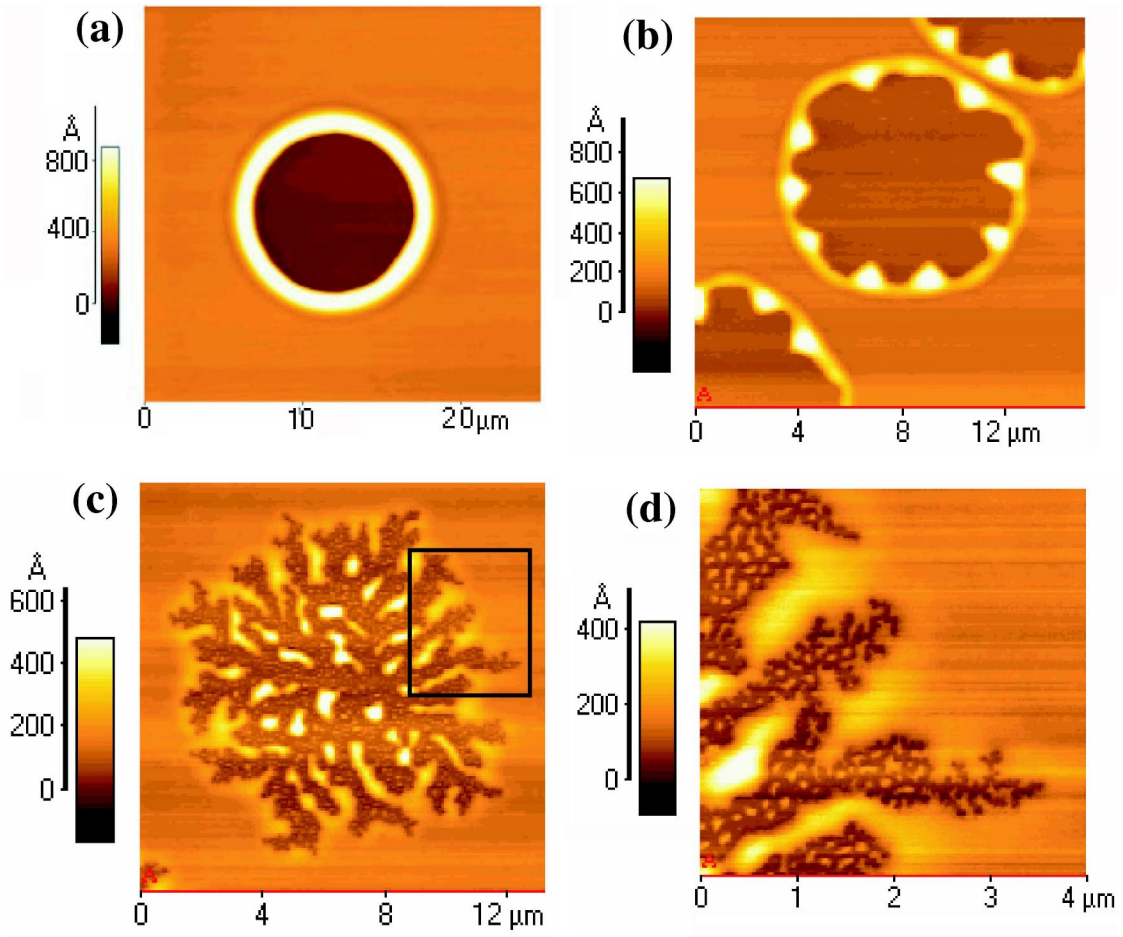

FIG. 1. (a) The circular holes of regime 1 resulting from a nucleation and growth process in a 32 nm 65 kg/mol film, (b) the simple fingering instabilities of regime 2 in an 11 nm 65 kg/mol PS film, (c) the dense radial structure of regime 3 in a 10 nm 290 kg/mol PS film, and (d) a magnification of the boxed region in (c) showing the random branching.

(in this case the slope) is sufficiently large, fingers develop. There exists a length scale over which the driving forces (gravitational forces, Marangoni forces, etc.) are balanced by the capillary forces and this length scale is assumed to be proportional to the wavelength between the fingers, λ [22–27]. It has been shown that λ is related to a capillary number Ca and to the film thickness h_0 [22–27],

$$\lambda \propto (\mathrm{Ca})^{-1/3} h_0, \tag{1}$$

where $\mathrm{Ca} = \eta V/\gamma$, η is the viscosity, γ is the surface tension, and V is the flow velocity of the liquid.

In this paper, we show that depending on the film thickness, growing holes in the $\mathrm{PS/Si/SiO}_x$ system may exhibit three distinct morphologies. For sufficiently thick films, the moving front of the hole remains circular (rim remains stable toward shape fluctuations) [Fig. 1(a)]; this is identified as the first regime and is well understood. For thinner films, fingers with a well-defined wavelength develop at the edge of holes after the holes become sufficiently large, as shown in Fig. 1(b) (regime 2). We show that the wavelength of these fingers can be described by Eq. (1) with appropriate modifications of V for the velocity of a growing hole. For the thinnest films (regime 3), random branching instabilities occur within the fingers [Figs. 1(c) and 1(d)]. The existence of this third regime is associated with the nature of the interactions between the chains and the substrate.

EXPERIMENT

We examined the dewetting of polystyrene films of varying thicknesses with molecular weights ranging from 65 to 290 kg/mol. The polystyrene standards were purchased from Pressure Chemical, Inc., and had polydispersities less than 1.06. The films were spun cast from toluene solution onto $\mathrm{Si/SiO}_x$ substrates purchased from Wafer World, Inc. that had a native oxide layer of 1.5 nm. After spin coating, the PS film thicknesses were measured using ellipsometry. The films were subsequently annealed above the glass transition temperature T_g at 170 °C under vacuum. Periodically, the samples were quenched to room temperature and imaged using an Autoprobe CP atomic force microscope (AFM) in contact mode.

As discussed in an earlier publication, fingering is preceded by a fluctuation in the shape of the rim and this occurs with a characteristic wavelength [20]. The wavelength was determined by measuring the average distance between the

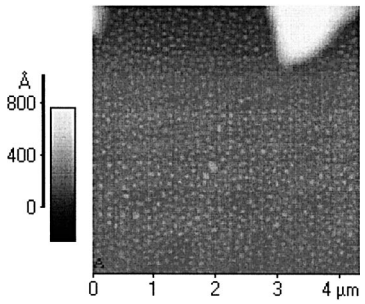

FIG. 2. Secondary droplets adsorbed to the substrate from a 290 kg/mol PS film are shown here in the vicinity of a larger droplet.

tips of the fingers using the linescan feature in the PSI Proscan Image Processing Software. Due to nonlinearities during the imaging process, the AFM images were flattened with second or third order whole image fits using the image processing before measurements were made. The average hole radius was determined by averaging the distance from the center of the hole to the fingers and the primary portion of the rim.

RESULTS AND DISCUSSION

The competition between short- and long-range intermolecular forces in the $PS/SiO_x/Si$ system produces an effective interface potential that exhibits a minimum at $h=L$ and exhibits a maximum at $h>L$ before decaying to zero at large h_0 [9–11]. The minimum at $h=L$ identifies a stable film thickness, the existence of which is due to the short-range interactions between the polymer and the substrate. Films thinner than L should, in principle, be stable whereas films thicker than L, in the thickness range defined by the negative curvature of the interface potential, should be unstable and dewet spinodally [9,10]. For sufficiently large thicknesses beyond the region of the interface potential with negative curvature, the films are metastable [10]. Films in this metastable regime become unstable via the nucleation, and subsequent growth, of holes when the energy barrier denoted by the maximum of the interface potential is overcome. In such a situation, holes would grow on the underlying layer of thickness L [11]. Eventually droplets would reside on this layer.

Experimentally, this underlying layer is found to be unstable and breaks up into secondary droplets. Consequently, a distribution of macroscopic droplets and microscopic, secondary, droplets comprise the final morphology. This is illustrated in Fig. 2. Based on self-consistent field (SCF) calculations, Müller *et al.* suggested that the thickness of this layer should be of order 2 nm, which they found to be in agreement with *in situ* x-ray reflectivity measurements of PS films of molecular weight 8700 g/mol [11]. They measured a mean secondary droplet height of 3 nm for the film in the unstable state. We investigated PS thin films with molecular weights ranging from $M=90$ to 1600 kg/mol on SiO_x/Si substrates and found that the mean height of the secondary droplets increased with increasing molecular weight. The

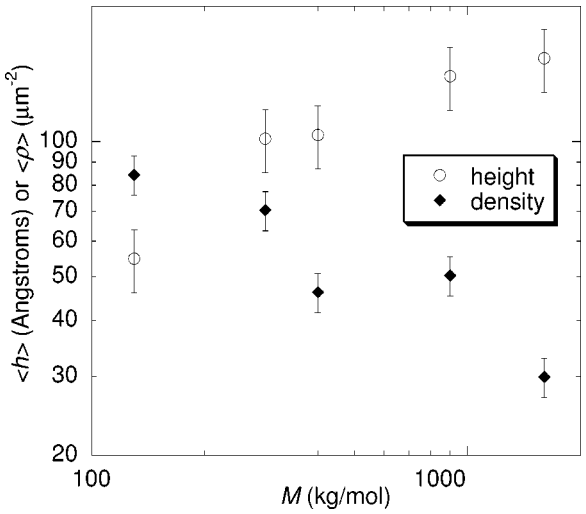

FIG. 3. The molecular weight dependence of the average secondary droplet height and secondary droplet density is shown.

droplet surface density was found to decrease with increasing molecular weight. These data are plotted in Fig. 3. These observations suggest that modifications of the theoretical effective interface potential, or alternative interface potentials, which account for effects associated with entropy (chain length, chain packing, and chain connectivity) and temperature would be required to fully describe these observations.

The existence of this secondary droplet layer appears to have an important effect on the morphology of sufficiently thin dewetting films. The satellite branching morphology which develops in the fingers is observed in films with thicknesses comparable to the height of the secondary droplets. For example, the films in Figs. 1(b) and 1(c) are, within experimental error, of the same thickness, except that the molecular weight of the film in Fig. 1(c) is $M=290$ kg/mol and that of the film in Fig. 1(b) is $M=65$ kg/mol. The secondary droplets are smaller for the lower molecular weight sample (Fig. 3). These results indicate that the ratio of the film thickness to the droplet size is of particular relevance and not the actual film thickness.

The morphology shown in Fig. 1(c) appears similar to the dense branching morphology (DBM) [28,29] or dense radial structure [30] commonly observed in radial Hele-Shaw cells. In the Hele-Shaw cell, a viscous fluid is placed between two circular parallel plates separated by a small distance [31,32]. An immiscible fluid with lower viscosity is then injected into the center of the top plate with an inlet pressure p_{inlet} displacing the high-viscosity fluid [28–32]. At intermediate inlet pressures, regular viscous fingering is observed whereas at high inlet pressures, random branching occurs [30]. In the latter, the DBM is characterized by a circular envelope with random branching from the main fingers. The DBM occurs as a result of the competition between the macroscopic diffusion field (the inlet pressure), which acts to destabilize the interface, and the effects of surface tension which act to smooth the interface [29].

Although the mechanism of random dense branching is different in Hele-Shaw cells, analogies to our system are worthwhile exploring. The presence of the secondary drop-

lets adsorbed to the substrate creates a low-mobility, high-viscosity layer (the chains are physisorbed to the substrate). This layer is unstable and forms droplets which are heterogeneously located on the SiO_x/Si substrate. The remainder of the film possesses a lower effective viscosity and associated higher mobility. Experimentally we find that for the thinnest films as a typical hole increases in size, fingers develop and the satellite instabilities develop in these fingers leading to the dense branching morphology. The pressure p at the line of contact is approximately $p=|S|/h_0$ [33,34], indicating that the pressure is greatest for the thinnest films in which the dense branching morphology is observed. These analogies to experiments performed in the Hele-Shaw cell indicate that there exists a competition between the pressure at the line of contact due to the capillary driving forces and the combined effects of surface tension and viscous dissipation at the substrate that act to stabilize the interface [29]. As the film thickness approaches the size of the secondary droplets, the pressure at the contact line due to the capillary driving forces becomes sufficiently large, and the dense branching morphology is observed.

In summary, it would therefore appear that three morphological regimes of instabilities are possible for films that dewet via nucleation and growth of holes. The first is characterized by the formation of circular holes; the second is characterized by fingers along the perimeter of the hole, and the third is a dense branchlike morphology along the perimeter of the hole, described heretofore. The dense branchlike morphology is difficult to quantify and we therefore turn our attention to the first two regimes. In the next section the dynamics of circular holes is discussed. While a great deal has been said about this, two essential points that have an important bearing on the behavior of holes in regime 2 are addressed, namely, the temporal dependencies of the hole radius R and the rim width w_R. The issue specifically concerns the role of slip in the dynamics of holes.

Dynamics of circular holes: Regime 1

The growth of circular holes (regime 1) along the substrate is driven by capillary forces (negative spreading coefficient) and opposed by viscous forces. As a hole grows, chains are excavated from the interior of the hole to form a rim, which increases in size with time. There exist two limiting cases that describe the growth of holes. In the first case, all of the energy is assumed to be dissipated in a wedge near the contact line and the hole grows linearly in time with a velocity specified by [1,35,36]

$$V=\frac{dR}{dt}=k\frac{\gamma}{\eta}\theta_E^3, \tag{2}$$

where γ is the surface tension, η is the viscosity, and θ is the contact angle. The hole grows at a constant rate in this situation because the capillary driving forces are balanced by the viscous resistive forces. Equation (2) indicates that the dewetting velocity is independent of the film thickness.

Alternatively, if the energy is dissipated primarily at the substrate over the width of the rim, the film slips along the substrate (i.e., a nonzero velocity at the substrate) and the viscous forces become dependent on the size of the growing rim [13,36–38]. In this scenario, when the rim is small and not fully developed, the velocity of the slipping film is constant [13],

$$V=\frac{|S|}{\eta}\left(\frac{b}{h_0}\right)^{1/2}, \tag{3}$$

where S is the spreading coefficient, h_0 is the initial film thickness, and b is the slip extrapolation parameter. The slip length b is determined by the viscosity η and the monomer friction coefficient k ($k=\eta/b$) [37]. During this interval, the rim width, w_R, increases as $t^{1/2}$ as expected from volume conservation [1,37].

Brochard *et al.* point out that after the initial linear growth stage ($R\propto t$) of the hole on the substrate, the hole radius then exhibits a power law dependence, $R\propto t^{2/3}$ [13]. The rim is not fully developed during the initial stages but becomes well developed during the latter stage where the increase of size of its width transitions from $t^{1/2}$ to $t^{1/3}$ [13]. Note that at sufficiently long times when the rim is particularly large, the growth rate eventually becomes constant again because the viscous resistance dominates. In short, at early times the slip process is characterized by two power law regimes, initially $R\propto t$ followed by $R\propto t^{2/3}$. Eventually, at long times, $R\propto t$ again.

We can examine the time dependence of the growth of the radius $R(t)$ and of the rim width of a hole $w(t)$ in a PS film on the substrate. Figure 4(a) shows a plot of the radius as a function of time, which is consistent with a transition from linear growth $R\propto t$ at early times to power law growth $R\propto t^{2/3}$ at later times. This transition occurs at a radius of approximately 3 μm, as indicated by the solid line. In addition, the temporal growth of the rim width exhibits a distinct transition from $t^{1/2}$ to $t^{1/3}$ growth, as shown in Fig. 4(b), at the same radius. Together these data clearly support the notion that a slip mechanism is operational during the early stage.

There is another prediction regarding the growth of holes on a substrate. Jacobs *et al.* have suggested that the two limiting mechanisms of slip and nonslip can occur simultaneously [39,40]. They indicate that at early times the slip process should be dominant and $R\propto t^{2/3}$, whereas at later times the nonslip mechanism should become dominant and $R\propto t$. By assuming that the velocities due to the individual cases of slip and nonslip are additive, they suggest the following relation between the time and the hole radius:

$$t(R)=\frac{K_v}{S}\left[R-2\gamma\sqrt{R}+2\gamma^2\ln\left(1+\frac{\sqrt{R}}{\gamma}\right)\right]+t_0. \tag{4}$$

In this equation, S is the spreading coefficient, t_0 is a rupture time associated with the nucleation stage, and K_v is the viscous dissipation constant. K_v depends on the contact angle and describes the total viscous dissipation within the rim for the nonslip case. It is defined by $K_v(\theta)=S/v_v$ where v_v is the dewetting velocity in the absence of slip [39]. The parameter γ is defined by $\gamma=K_v/K_s$ where K_s is the slippage constant, which is directly proportional to the friction coefficient [40]. The slippage constant is defined by $K_s=S/v_s\sqrt{R}$ where v_s is the hole growth velocity for the slip process [39]. The pa-

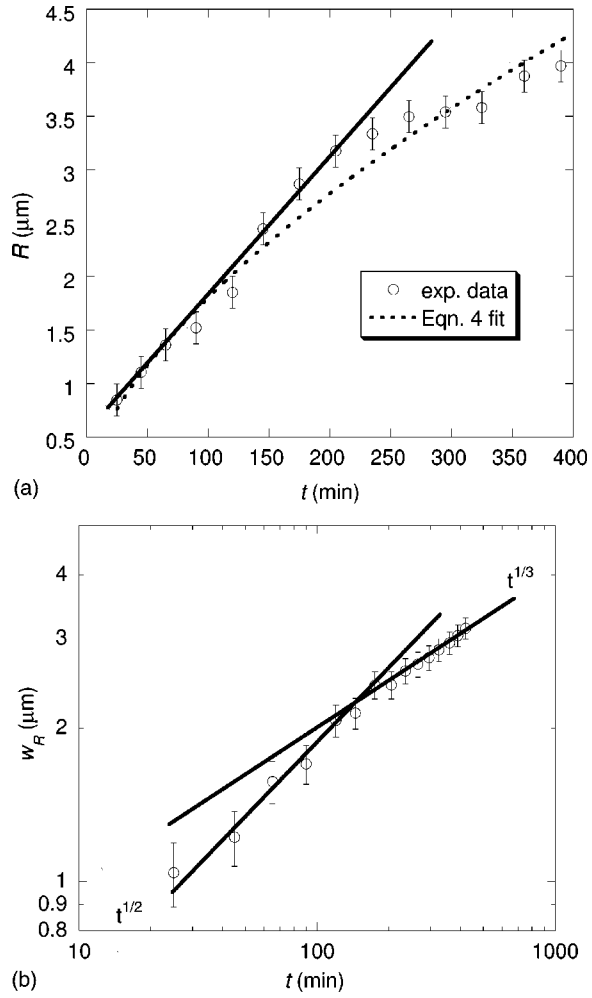

FIG. 4. (a) The radius of a 34 nm 152 kg/mol film is plotted as a function of time showing the turnover to power law growth and (b) the corresponding transition of the rim width from $t^{1/2}$ to $t^{1/3}$ growth indicative of slippage.

rameter γ provides an indication of the relative modes of dissipation during the dewetting process. The full slippage case is recovered when $\gamma=\infty$ and the nonslip case is recovered when $\gamma=0$. Equation (4) indicates that at short times, the dominant mechanism of dissipation is slippage while at later times and large hole sizes, viscous effects within the film dominate the dissipation process [39].

The role of slip in the dewetting process can be examined by fitting Eq. (4) to the hole growth data of Fig. 4(a). For PS on Si/SiO_x, the equilibrium contact angle is 35°, which sets $|S|=5.75$ mJ/m^2 [18]. A fit to the data, shown by the dotted line in Fig. 4(a), yielded the values of $K_v=7.39\times10^7$ Pa s m$^{-1/2}$, $K_s=4.53\times10^{10}$ Pa s ($\gamma=1.63\times10^{-3}$ m$^{1/2}$), and $t_0=-23$ min. Adequate fits to the data were not obtainable with $t_0\geqslant0$ unless γ was increased to unusually large values. The margin of uncertainty of the fits of this equation to our data would be expected to be large since our data are limited in range (we are specifically interested in the early stages). Jacobs *et al.* appeared to get better fits to their data (Refs. [39,40]) because they tracked the time dependence of their holes to larger times where the velocities became constant (i.e., they note a transition from $R\propto t^{2/3}$ to $R\propto t$ at long times). Nevertheless, although the fit of Eq. (4) to our data was not very good, the values of γ extracted from the fits increased rapidly with increasing molecular weight, consistent with the viscosity, as one would expect [42]. The basic conclusion from this analysis, using Eq. (4), is consistent with the assessment using the Brochard analysis [13,41]. Our assessment based on the latter predictions indicates that the slip length in this system is considerably smaller than a theoretical value based on complete slip (i.e., partial slip). This reduction of the slippage length, or equivalently partial slip, is likely due to the adsorption of chains to the substrate.

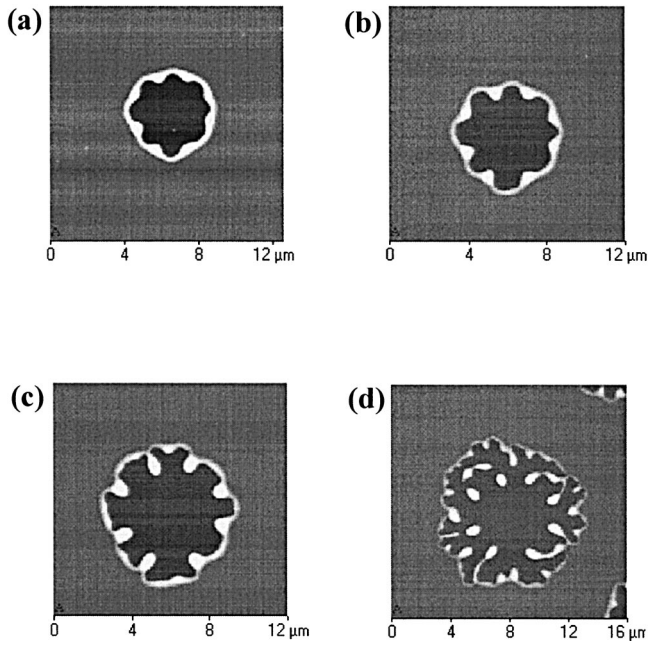

FIG. 5. The temporal development of the fingering instability in a film of initial thickness $h_0=10$ nm ($M=90$ kg/mol) is shown here for times of (a) 8, (b) 13, (c) 18, and (d) 23 min.

Growth of fingers: Regime 2

In regime 2, the fingers that initially develop along the perimeter of the hole are separated by a well defined wavelength. Mechanistically, as the hole grows, fluctuations in the rim height spontaneously develop. As a result of these fluctuations, a Laplace pressure gradient is established in the rim due to the local variations in curvature, which drives material from thicker to thinner regions in order to stabilize the fluctuations. However, the thinner regions of the rim between the fingers move at a faster rate than the thicker regions because the thinner regions provide less resistance to the capillary driving forces [20,38]. The result is the formation of fingers.

The process of finger formation is illustrated in Figs. 5(a)–5(c). As the hole grows, the spacing between the fingers at the rim increases. When this spacing is sufficiently large, secondary instabilities begin to develop between the fingers of the initial instability as shown in Fig. 5(c). As the hole continues to grow, the primary fingers increase in length and eventually detach from the rim [20,21], and the fingers typi-

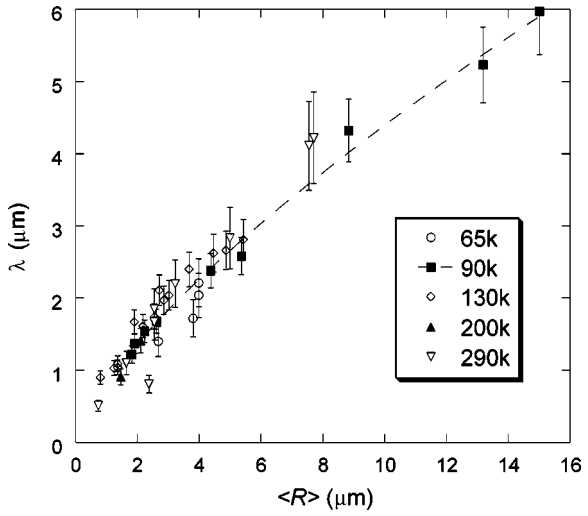

FIG. 6. The wavelength of the instability, λ, is shown here to be dependent on $\langle R \rangle$ for all initial film thicknesses and molecular weights.

cally break up to form droplets, as shown in Fig. 5(d) [19]. Of particular interest in our subsequent analysis is the formation of the fingers as a result of the primary instability.

The remainder of this section concerns the instability associated with the formation of the primary fingers. The wavelength between primary fingers increases with increasing hole size. These wavelengths are plotted in Fig. 6 as a function of the average hole radius $\langle R \rangle$ for all film thicknesses and molecular weights studied. These data collapse onto one curve and indicate that $\lambda \propto \langle R \rangle^{0.7}$. The wavelength in the radial geometry is essentially an arc length on a circle. This arc length is inversely proportional to the number of fingers, N_f, in the hole. If the number of fingers remained constant for all films, one would expect the wavelength to be proportional to $\langle R \rangle$, which is not observed here.

The data in Fig. 7 indicate that in fact the number of fingers from the primary instability depends on the initial film thickness and on molecular weight. The AFM images in Figs. 1(b) and 5(b) show a distinct difference between morphologies for two different molecular weight samples of the same initial thickness; the number of fingers and the distance between fingers differ. The value of the wavelength varies for different molecular weights at a constant h_0 because the rims in higher molecular weight films become unstable at smaller critical radii. The fingers develop when the holes grow beyond a critical size. This is shown in Fig. 8 where critical radii are shown to increase with h_0 and to decrease with increasing M.

A characteristic length scale over which the capillary forces are balanced by the viscous resistive forces was defined in the same manner as the situation involving small molecule liquids ("driven flows") [22–27]. This length scale was assumed to be proportional to the wavelength of the instability and an equation identical in form to Eq. (1) was derived [20]. As demonstrated in Fig. 4, the velocity of hole growth is described by Eq. (3). Inserting Eq. (3) (and using the theoretical expression for the slip extrapolation parameter, $b \propto M^3/M_e^2$ [36]) into the capillary number in Eq. (1) yields

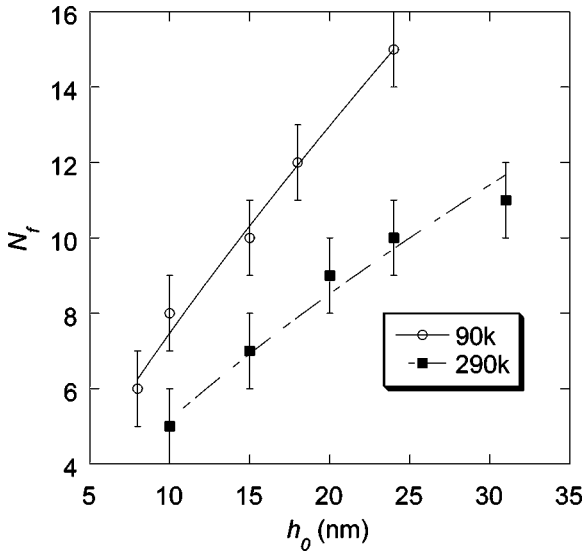

FIG. 7. The number of fingers in the primary instability is shown here as a function of film thickness and molecular weight. For clarity, only the $M = 90$ and 290 kg/mol samples are shown.

$$\lambda \propto \left(\frac{M_e \gamma}{|S|} \right)^{1/3} \frac{h_0^{7/6}}{M^{1/2}}, \tag{5}$$

where M_e is the molecular weight between entanglements [20]. This equation suggests a connection between λ, the initial film thickness h_0, and the molecular weight M. A plot of $\lambda M^{1/2}$ versus $h_0^{7/6}$ is shown in Fig. 9. All the data collapse onto one curve in a manner consistent with Eq. (5). Note that if slip was assumed to be absent, then the velocity would be specified by Eq. (2) and the wavelength would be predicted to be

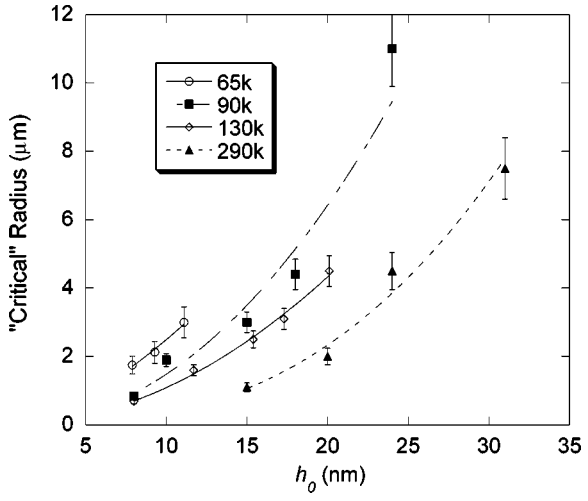

FIG. 8. The "critical" radius for finger formation is plotted as a function of film thickness. The "critical" radius is determined when the amplitude of the fingers, or the distance from which the fingers protrude from the main portion of the rim, is comparable to the rim width as shown in Fig. 1(b). This distance varies with film thickness and is typically between 0.5 and 2 μm.

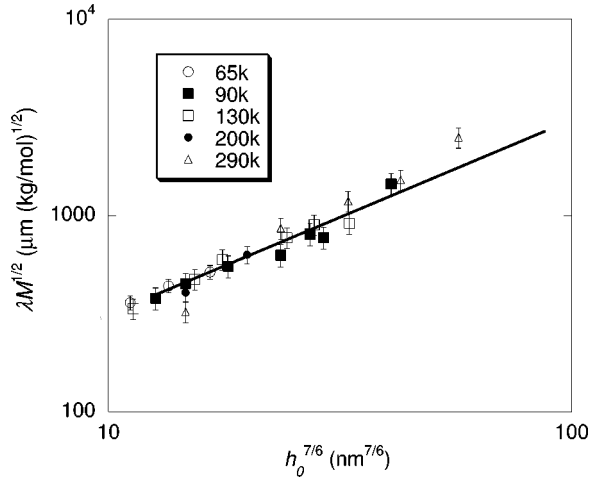

FIG. 9. The parameter $\lambda M^{1/2}$ is shown here to be proportional to $h_0^{7/6}$.

$$\lambda \propto \frac{h_0}{\theta_e}. \tag{6}$$

This equation indicates that the wavelength is not a function of molecular weight, whereas the data in Fig. 9 indicate that $\lambda \propto M^{-1/2}$. Therefore, Eq. (6) is inconsistent with our findings.

It is clear, thus far, and indeed from the work of Masson *et al.* that there exists a threshold thickness beyond which the holes remain circular and fingers are not observed [20]. This threshold film thickness increases with increasing molecular weight. In light of this observation, it is tempting to suggest that the phenomenon is suppressed in thicker films. On the contrary, the instability is, in fact, not suppressed, in thicker films. We see fingering instabilities develop at the edges of films (scratched prior to annealing) which are thicker than the threshold thickness observed for fingering in holes. One should then, in principle, expect fingering instabilities to occur if an isolated hole were allowed to grow unimpeded. However, the density of holes has been shown to scale as h_0^{-2} [1,4]. This suggests that in thicker films the density of holes is much smaller compared to thinner films and so each hole, in principle, should have sufficient opportunity to experience the instability. On the other hand, as shown by our data (Fig. 8), the "critical" radius for finger formation scales roughly as $R_c \propto h_0^2/M^\alpha$ (where $\alpha \sim 0.8$). The apparent chain length dependence of the threshold film thickness is associated with the fact that the "critical" hole radius exhibits a molecular weight dependence $M^{-0.8}$. In light of the critical hole size dependence on h_0 and the dependence of the density on h_0, and the fact that fingers are observed at the edge of thick films, the situation involving the suppression of the phenomenon in circular holes is not entirely clear-cut. Experimentally we find that the rims of holes in the threshold regime fluctuate but the holes impinge before the formation of fingers.

CONCLUDING REMARKS

Thin (~nanometers) supported liquid films can become unstable via two different mechanisms, nucleation and growth or a spinodal process. We showed that with regard to the nucleation and growth mechanism, the growing holes in the $PS/SiO_x/Si$ systems exhibit three distinct morphologies, depending on film thickness. During the hole growth process, a rim, into which chains accumulate, develops at the periphery of the growing hole. In sufficiently thick films, the holes remain circular during growth. Eventually the holes impinge, leading to a series of droplets which reside on a thin layer of secondary droplets (regime 1). In thinner films, the fluctuations in the rims become unstable and form fingers (regime 2). The wavelength of the fingers along the perimeter of the holes depends on molecular weight and initial film thickness, $\lambda \propto h_0^{7/6}/M^{1/2}$. There exists an apparent threshold film thickness, beyond which the fingers are not observed, which increases with M. This is due to the fact that the holes grow to a "critical" size before the fluctuations are sufficiently large and this critical size depends on the molecular weight of the polymer. For sufficiently thin films, with thicknesses comparable to the size of the secondary droplets, the holes exhibit a branchlike morphology. In this latter regime, regime 3, the hole growth velocity is largest; it increases strongly with decreasing film thickness.

A comprehensive theoretical picture of the instabilities described here is yet to emerge and it is hoped that these experiments will serve as a basis for further theory on this topic. An important additional issue evolves around the role of interfacial interactions on the morphological development in such systems.

ACKNOWLEDGMENTS

This work was supported by the National Science Foundation (Grant No. DMR9705101) and the Robert A. Welch Foundation. Helpful discussions with Venkat Ganesan are gratefully acknowledged.

[1] F. Brochard-Wyart and J. Daillant, Can. J. Phys. **68**, 1084 (1990).
[2] H. S. Kheshgi and L. E. Scriven, Chem. Eng. Sci. **46**, 519 (1991).
[3] G. Reiter, Phys. Rev. Lett. **68**, 75 (1992).
[4] G. Reiter, Langmuir **9**, 1344 (1993).
[5] R. Segalman and P. F. Green, Macromolecules **32**, 801 (1999).
[6] J.-L. Masson and P. F. Green, J. Chem. Phys. **112**, 349 (2000).
[7] R. Limary and P. F. Green, Langmuir **15**, 5617 (1999).
[8] R. Xie, A. Karim, J. F. Douglas, C. C. Han, and R. A. Weiss, Phys. Rev. Lett. **81**, 1251 (1998).
[9] A. Sharma and R. Khanna, Phys. Rev. Lett. **81**, 3463 (1998).
[10] R. Seemann, S. Herminghaus, and K. Jacobs, Phys. Rev. Lett. **86**, 5534 (2001).

[11] M. Müller, L. G. MacDowell, P. Müller-Buschbaum, O. Wunnike, and M. Stamm, J. Chem. Phys. **115**, 9960 (2001).
[12] J. Israelachvili, *Intermolecular Surface Forces*, 2nd ed. (Academic, New York, 1992).
[13] F. Brochard-Wyart, G. Debregeas, R. Fondecave, and P. Martin, Macromolecules **30**, 1211 (1997).
[14] K. Jacobs, S. Herminghaus, and K. R. Mecke, Langmuir **14**, 965 (1998).
[15] R. Seemann, S. Herminghaus, and K. Jacobs, Phys. Rev. Lett. **87**, 196101 (2001).
[16] S. Herminghaus, R. Seemann, and K. Jacobs, Phys. Rev. Lett. **89**, 056101 (2002).
[17] J.-L. Masson and P. F. Green, Phys. Rev. Lett. **88**, 205504 (2002).
[18] J.-L. Masson and P. F. Green, Phys. Rev. E **65**, 031806 (2002).
[19] F. Brochard-Wyart and C. Redon, Langmuir **8**, 2324 (1992).
[20] J.-L. Masson, O. Olufokunbi, and P. F. Green, Macromolecules **35**, 6992 (2002).
[21] G. Reiter and A. Sharma, Phys. Rev. Lett. **87**, 166103 (2001).
[22] H. E. Huppert, Nature (London) **300**, 427 (1982).
[23] S. M. Troian, E. Herbolzheimer, S. A. Safran, and J. F. Joanny, Europhys. Lett. **10**, 25 (1989).
[24] M. A. Spaid and G. M. Homsy, Phys. Fluids **8**, 460 (1996).
[25] A. L. Bertozzi and M. P. Brenner, Phys. Fluids **9**, 530 (1997).
[26] F. Melo, J. F. Joanny, and S. Fauve, Phys. Rev. Lett. **63**, 1958 (1989).
[27] A. M. Cazabat, F. Heslot, S. M. Troian, and P. Carles, Nature (London) **346**, 824 (1990).
[28] E. Ben-Jacob, G. Deutscher, P. Garik, N. D. Goldenfeld, and Y. Lareah, Phys. Rev. Lett. **57**, 1903 (1986).
[29] E. Ben-Jacob and P. Garik, Nature (London) **343**, 523 (1990).
[30] T. Vicsek, *Fractal Growth Phenomena* (World Scientific, Singapore, 1989).
[31] L. Paterson, J. Fluid Mech. **113**, 513 (1981).
[32] L. Paterson, Phys. Fluids **28**, 26 (1985).
[33] G. Debregeas, P. Martin, and F. Brochard-Wyart, Phys. Rev. Lett. **75**, 3886 (1995).
[34] G. Reiter, Phys. Rev. Lett. **87**, 186101 (2001).
[35] C. Redon, F. Brochard-Wyart, and F. Rondelez, Phys. Rev. Lett. **66**, 715 (1991).
[36] P. G. de Gennes, Rev. Mod. Phys. **57**, 827 (1985).
[37] F. Brochard-Wyart, P. G. de Gennes, H. Hervert, and C. Redon, Langmuir **10**, 1566 (1994).
[38] C. Redon, J. B. Brzoska, and F. Brochard-Wyart, Macromolecules **27**, 468 (1994).
[39] K. Jacobs, R. Seemann, G. Schatz, and S. Herminghaus, Langmuir **14**, 4961 (1998).
[40] C. Neto and K. Jacobs, Physica A **339**, 66 (2004).
[41] P. F. Green and V. Ganesan, Eur. Phys. J. E **12**, 449 (2003).
[42] For films of thickness $h_0=32$ nm, with molecular weights 65, 152, and 290 kg/mol, values of $\gamma=5\times10^{-5}$ ($t_o=5.9$ min), 1.6×10^{-3} ($t_o=-23$ min), and 8.5×10^{-3} ($t_o=-119$ min), respectively, were extracted. In our experiments $t=0$ was the time the sample was initially placed in the oven. Regardless of whether the early-time or later-time data sets is emphasized in the fits, the basic conclusion stands: a partial slip mechanism is operational.